Atomic-scale self-organization of Fe nanostripes on stepped Cu(111) surfaces: Molecular dynamics and kinetic Monte Carlo simulations

N. N. Negulyaev,[1] V. S. Stepanyuk,[2] W. Hergert,[1] P. Bruno,[2] and J. Kirschner[2]

[1]*Fachbereich Physik, Martin-Luther-Universität Halle-Wittenberg, Friedemann-Bach-Platz 6, D-06099 Halle, Germany*
[2]*Max-Planck-Institut für Mikrostrukturphysik, Weinberg 2, D-06120 Halle, Germany*

Growth of Fe nanostripes on a vicinal Cu(111) surface is investigated on the atomic scale by performing molecular dynamics and kinetic Monte Carlo simulations. We involve in our study the kinetic mechanisms of atomic incorporation recently reported by Mo *et al.* [Phys. Rev. Lett. **94**, 155503 (2005)]. The atomistic processes responsible for the interlayer mass transport and the formation of Fe stripes of 1 ML height are identified. We demonstrate that strain relaxations at steps have a strong impact on the self-assembly of one-dimensional Fe atomic structures on vicinal Cu(111).

PACS number(s): 61.46.−w

I. INTRODUCTION

Fabrication of stable magnetic one-dimensional (1D) nanostructures is a challenge for modern nanoscience. This interest originated from the intriguing magnetic properties, which are peculiar to 1D systems.[1] The most obvious way of 1D nanostructure formation is to use a stepped substrate. The idea to utilize the ascending steps as nucleation centers for the deposited atoms was proposed by Bassett[2] and Bethge[3] 50 years ago. They revealed that metal atoms deposited on nonmetal substrates are trapped by the ascending steps and aggregate into compact clusters along the steps. The first clear evidence that the step-flow mechanism can be exploited for the fabrication of the 1D nanostructures was obtained in the experiments of Brodde *et al.*,[4] who found that Fe atoms deposited on a Cu(111) surface were self-assembled into long atomic stripes decorating step edges. Studies of Elmers *et al.*[5] demonstrated that Fe atoms evaporated onto vicinal W(110) form a system of parallel atomic stripes along the ascending steps. In the experiments of Himpsel and co-workers,[6] different combinations of "deposit" and "substrate" materials were investigated and several new systems exhibiting growth of ordered atomic stripes were revealed. On the vicinal Cu(111) surface, an array of parallel Fe stripes was produced in the experiments of Shen *et al.*[7,8] Recently, parallel rows of monatomic Co wires on vicinal Pt(997) have been fabricated by Gambardella *et al.*[9,10] Later on, Shiraki *et al.*[11] have demonstrated that Fe atoms may self-assemble into monatomic chains on Au(111).

Usually, nanowires or nanostripes grow on lower terraces along an ascending step edge. Surprisingly, the observations of Shen *et al.*[7,8] have demonstrated that Fe nanostripes grow on the upper terrace of a stepped Cu(111) surface. For almost ten years, which kind of kinetic mechanism leads to the formation of such structures has been a puzzle. An important step was made by Mo *et al.*, who used total-energy calculations within the density functional theory and showed that the growth of Fe nanowires is a two-stage process.[12] First, Fe adatoms form an atomic row incorporated into the Cu substrate one lateral lattice constant away from the descending step. Then, the embedded Fe row acts as an attractor for the second row of Fe atoms. Very recently, Guo *et al.* have ex-

perimentally confirmed this growth scenario.[13] The kinetic Monte Carlo (kMC) simulations[14] based on atomic processes predicted by Mo *et al.*[12] have shown the existence of an optimal temperature and deposition flux for the formation of well-ordered Fe nanowires on stepped Cu(111) surfaces. These simulations have assumed only the growth of 1 ML high stripes. However, the interlayer mass transport between the lower and upper terraces and adatom diffusion on top of the stripes are important processes which could significantly affect the growth of Fe stripes.

In this paper, we report on detailed atomic-scale simulations of the 1D Fe nanostructure formation on a stepped Cu(111) surface. The first goal of our work is to study the effect of the interlayer mass transport on the formation of Fe stripes. The second goal is to demonstrate that atomic relaxations at steps significantly affect the initial growth of Fe nanowires and nanostripes.

The paper has the following structure. In Sec. II, we describe the molecular dynamics–kinetic Monte Carlo (MD-kMC) model used for our simulations. In Sec. III, we reveal basic atomic processes responsible for the growth of Fe nanostripes and demonstrate the results of kMC simulations. In Sec. IV, we discuss our results: we investigate the role of temperature, coverage, and strain relaxations at steps in the self-organization of atomic Fe stripes on stepped Cu(111).

II. MOLECULAR DYNAMICS–KINETIC MONTE CARLO MODEL

To perform large-scale atomic simulations, we use a combination of MD and kMC methods. *Ab initio* database for fitting and testing interatomic potentials are used in our work, as was proposed in several studies on nonmagnetic and magnetic systems.[15–20] In the present work, interatomic potentials are formulated in the second moment of the tight-binding (TB) approximation.[21] Previous studies[22–28] have demonstrated that the combination of *ab initio* and tight-binding methods allows one to construct many-body potentials for low-dimensional structures and to study large systems in fully relaxed geometries.

In TB approximation, the attractive term (band energy) E_B^i contains the many-body interaction. The repulsive part E_R^i is

TH-2008-04

TABLE I. Data used for the fitting of Fe-Cu and Fe-Fe potentials and the corresponding values computed with the optimized potentials. Bulk properties of Fe (lattice constant a_{Fe}, cohesive energy E_C, and bulk modulus B) are taken from Ref. 20. The atomic configurations of small embedded and supported Fe clusters, used for the fitting procedure, are shown in Fig. 1.

	Quantity	Configuration (Fig. 1)	Data	Fitted value
Fe	a_{Fe} (Å)		2.87	2.90
(bcc)	E_C (eV)		4.29	4.40
	B (Mbar)		1.69	1.32
Fe-Cu	$E_{dim,111}^{emb}$ (eV)	1	−0.24	−0.27
	$E_{trm,111}^{emb}$ (eV)	2	−0.69	−0.66
	$E_{2\times2,111}^{emb}$ (eV)	3	−1.02	−1.03
	$E_{dim,111}^{sup}$ (eV)	4	−1.21	−1.17
	$E_{trm,111}^{sup}$ (eV)	5	−3.45	−2.91
	$E_{dim,001}^{emb}$ (eV)	6	−0.32	−0.32
	$E_{dim,001}^{sup}$ (eV)	7	−1.15	−1.05
	$E_{trm,001}^{sup}$ (eV)	8	−2.06	−1.95
	$E_{2\times2,001}^{sup}$ (eV)	9	−4.17	−3.87
	$E_{4\times1,001}^{sup}$ (eV)	10	−3.03	−2.84

described by pair interactions (Born-Mayer form).[21,29] The cohesive energy E_{tot} is the sum of the band energy and repulsive part:

$$E_{tot} = \sum_i (E_R^i + E_B^i), \quad (1)$$

$$E_R^i = \sum_j \left[A_{\alpha\beta}^1 \left(\frac{r_{ij}}{r_0^{\alpha\beta}} - 1 \right) + A_{\alpha\beta}^0 \right] \exp\left[-p_{\alpha\beta} \left(\frac{r_{ij}}{r_0^{\alpha\beta}} - 1 \right) \right], \quad (2)$$

$$E_B^i = -\left\{ \sum_j \xi_{\alpha\beta}^2 \exp\left[-2q_{\alpha\beta} \left(\frac{r_{ij}}{r_0^{\alpha\beta}} - 1 \right) \right] \right\}^{1/2}, \quad (3)$$

where r_{ij} is the distance between the atoms i and j, $r_0^{\alpha\beta}$ is an adjustable parameter, $\xi_{\alpha\beta}$ is an effective hopping integral, and parameters $q_{\alpha\beta}$ and $p_{\alpha\beta}$ describe the decay of the interaction strength with distance between atoms.

The parameters of Cu-Cu interaction are taken from Ref. 29. They were fitted to experimental data for bulk Cu (lattice constant, cohesive energy, bulk modulus, elastic constants). The database for fitting Fe-Fe and Fe-Cu parameters includes the following data covering a variety of different structures: bulk properties of bcc Fe and binding energies of different clusters supported and embedded on Cu(111) and Cu(001) (Table I, Fig. 1). We apply the Korringa-Kohn-Rostoker Green's function method[30,31] to calculate the binding energies of the following clusters on Cu(111) (Fig. 1, configurations 1–5): embedded dimer $E_{dim,111}^{emb}$, embedded compact trimer $E_{trm,111}^{emb}$, embedded cluster of four atoms $E_{2\times2,111}^{emb}$, supported dimer $E_{dim,111}^{sup}$, and supported compact trimer $E_{trm,111}^{sup}$. On Cu(001), we calculate the binding energies of embedded dimer $E_{dim,001}^{emb}$, supported dimer $E_{dim,001}^{sup}$, supported
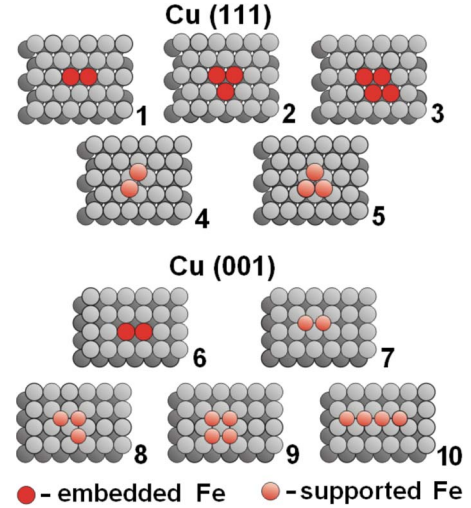

FIG. 1. (Color online) Small embedded and supported Fe clusters on Cu(111) and Cu(001), which are used to fit many-body interatomic potentials.

compact trimer $E_{trm,001}^{sup}$, supported cluster of four atoms $E_{2\times2,001}^{sup}$, and supported chain of four atoms $E_{4\times1,001}^{sup}$ (Fig. 1, configurations 6–10). In our calculations, magnetic effects are included implicitly by performing the spin-polarized calculations for all clusters. Note that recently, new magnetic potentials for iron have been proposed.[32] However, to our knowledge, only calculations for a bulk phase have been done and these potentials are still under discussion.[20]

The set of data used to define potentials and the corresponding values calculated by means of the optimized potentials are presented in Table I. The parameters of interatomic interactions are given in Table II.

To demonstrate that our potentials can describe with good accuracy the surface properties at the Fe/Cu interface not included in a fitting, we calculate displacements of Fe adatoms and Fe monolayers on Cu(111) and Cu(001) from their ideal positions and also diffusion barriers for Fe adatom on both substrates. We compare these results with the calculations by the VASP code[34] (see Table III). The details of our VASP calculations are similar to those reported in Ref. 12. On both Cu(111) and Cu(001) surfaces, we consider the relative vertical displacement d_1/d_0 of Fe adatom placed in the hollow site,[35] the activation energy required for the adatom to reach saddle point E_D (i.e., diffusion barrier of monomer), and the relative vertical displacement d_2/d_0 of 1 ML of Fe

TABLE II. Parameters of interatomic potentials.

Parameter	Cu-Cu	Fe-Fe	Fe-Cu
A^1 (eV)	0.0	−0.777	−1.909
A^0 (eV)	0.086	0.162	−0.026
ξ (eV)	1.224	1.573	0.881
p	10.939	5.872	7.148
q	2.280	2.105	5.178
r_0 (Å)	2.556	2.474	2.441

TABLE III. Data used to test the validity of the optimized potentials: the results of calculations using the VASP code (Ref. 34) together with the values computed within the MD simulations using many-body interatomic potentials (Table II).

Quantity	Cu(111)		Cu(001)	
	MD	VASP	MD	VASP
d_1/d_0	0.864	0.868	0.855	0.852
E_D (eV)	0.025	0.022	0.58	0.55
d_2/d_0	0.994	1.004	0.994	0.998

located on top of the substrate (Fig. 2). The results presented in Table III indicate that the interatomic potentials (Table II) give a good description of the energetics and relaxations at the Fe/Cu interface.

A vast amount of different atomic processes is considered in the framework of our MD-kMC model: step-flow diffusion, corner mass transport, and interlayer diffusion of Fe and Cu atoms between the lower and upper terraces and the top of the growing stripes. Activation barriers for the direct crossing of a step and stripe edge (in both upward and downward directions)[36,37] are rather high, as soon as a migrating atom reduces the bonds to all its neighbors during the crossing. Therefore, it is of essential importance to include exchange processes at the step edges. The energy barriers for the atomic transitions are computed by means of the MD, where the positions of Fe and substrate atoms are determined in fully relaxed geometry. The slab consists of ten layers with 1020 atoms in each layer. Two bottom layers are fixed. Periodic boundary conditions are applied in the surface plane. The cutoff radius for the interatomic potentials is set to 6.0 Å.

We employ the general kMC method introduced by Fichthorn and Weinberg[38] and used in a number of recent publications.[14,39–43] According to this approach, the frequency v of the considered atomic transition is calculated within the ratio $v = v_0 \exp(-E_D/k_BT)$, where E_D is the activation barrier, T is the temperature, k_B is the Boltzmann constant, and v_0 is the prefactor. For all atomic transitions v_0 is taken to be 10^{12} Hz.[39–43] We follow the experimental setup of Shen et al.[7,8] and set the flux F to 0.2 ML/min and the temperature T to 273 K. The width of the terrace of the stepped Cu(111) surface is set to 10 nm. The kMC simulations are carried out on a 392×452 atom close-packed (111) lattice (100×100 nm).

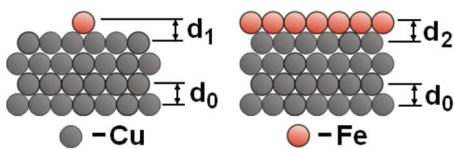The submonolayer deposition regime (with a characteristic coverage $D \sim 0.1$ ML) is examined. Therefore, the char-

acteristic time scale t_c of the evolution process is $D/F \sim 10$ s. Within the kMC model, the average transition time t_D of one atomic configuration to another one can be estimated using the expression $t_D \sim v_0^{-1} \exp(E_D/k_BT)$, where $v_0 = 10^{12}$ Hz and $k_B = 0.086$ meV/K. The examined event is operative only if $t_D < t_c$; otherwise, it is suppressed. In other words, all atomistic processes having activation barriers $E_D > E_{cr} = 0.7$ eV are inhibited at $T = 273$ K and $F = 0.2$ ML/min (examined temperature and flux). During our study, we compare the energy barriers of all atomistic processes with this threshold barrier. When the temperature decreases (increases), the magnitude of E_{cr} decreases (increases) as well.

On a fcc(111) stepped surface, two different kinds of close-packed steps can be distinguished: the (100)-microfaceted step (A step) and the (111)-microfaceted step (B step). The difference in the free energy of these two steps leads to the anisotropy in the potential energy landscapes for the atomic diffusion along the step edges and near corners and for exchange at step edges. In our paper, we concentrate on the B step; however, our studies indicate that self-assembly of Fe atoms along the A step is caused by similar atomic mechanisms.

III. RESULTS

In this section, we concentrate on the growth of 1D Fe nanostructures: we reveal basic atomic processes, responsible for the growth of stripes, and present the results of kMC simulations.

As has been shown by Mo et al.[12] and Guo et al.,[13] deposited Fe atoms are first embedded into the flat Cu(111) terrace at one atomic distance away from the upper edge of a step. Such embedded Fe wires serve as one-dimensional nucleation lines for the formation of monatomic Fe chains along the upper edges of the step. We have performed kMC simulations with the full set of atomic processes presented in the work of Mo et al. (see Figs. 1 and 2 in Ref. 12). Figure 3 depicts our results for a stepped Cu(111) surface covered by 0.045 ML of Fe atoms. In agreement with the experimental observations of Guo et al.,[13] our simulations clearly demonstrate that, first, a chain of embedded Fe atoms is formed one lateral lattice constant away from the descending Cu step. Subsequently, another chain of Fe atoms grows on top of that.

To understand the mechanism of nanostripe formation on the atomic scale, one needs to consider the dominant processes which occur near such monatomic wires. We incorporate these processes in the kMC simulation on time and length scales relevant for the experiment of Shen et al.[7,8] We used fully relaxed atomic configurations to determine the activation barriers for each of the elementary processes involved.

Due to the diffusive motion of Fe atoms on the terraces of a stepped Cu(111) surface, one-half of the deposited Fe adatoms reach a step edge from the upper terrace, while the second half reach from the lower one. First, we concentrate on the behavior of Fe adatoms approaching the step from the lower terrace (Figs. 4–6); further, we proceed to the behavior
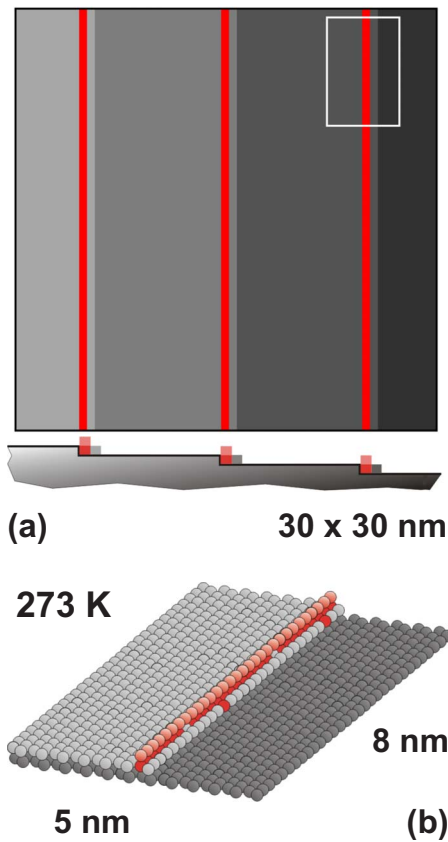

FIG. 2. (Color online) The vertical distances between Fe adatom (monolayer) and a substrate, exploited to test the optimized interatomic potentials.

(a)   30 x 30 nm

273 K

8 nm

5 nm   (b)

FIG. 3. (Color online) kMC simulation of the morphology of a stepped Cu(111) surface exposed to 0.045 ML of Fe atoms (T =273 K, F=0.2 ML/min). Fe atoms self-assemble into monatomic wires on top of embedded Fe rows. Snapshot (b) shows an enlarged view of the rectangle in (a). Red and gray colors represent Fe and Cu atoms, respectively.

of Fe approaching from the upper terrace (Fig. 7).

An Fe atom [Fig. 4(a)] has to overcome a barrier of 0.65 eV to ascend to the upper terrace by direct hopping over the step.[44] Though this process is operative at room tempera-
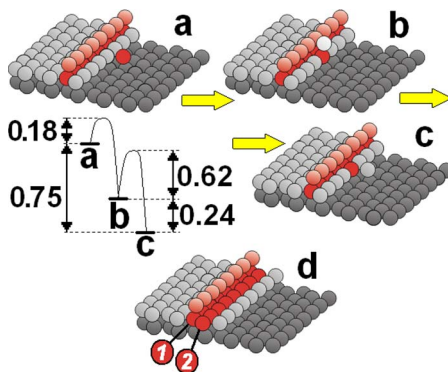

FIG. 4. (Color online) Transition $a \rightarrow b \rightarrow c$ is responsible for the growth of the second row of embedded Fe atoms (configuration d). The energy differences between the atomic configurations a, b, c and the values of activation barriers (in eV) are shown. Red and gray colors represent Fe and Cu atoms, respectively. Numbers 1 and 2 indicate the numbers of consecutively formed rows of Fe atoms embedded into the upper terrace.
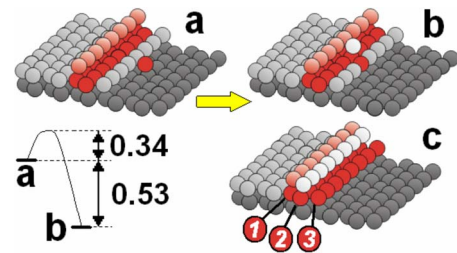

FIG. 5. (Color online) Transition $a \rightarrow b$ is responsible for the growth of the third row of embedded Fe atoms (configuration c) attached to the step edge. The energy differences between the atomic configurations a, b and the value of the activation barrier (in eV) are shown. Red and gray colors represent Fe and Cu atoms, respectively. Numbers 1–3 indicate the numbers of consecutively formed rows of Fe atoms embedded into the upper terrace.

ture, the Fe atom would prefer to incorporate itself into the step edge by means of the exchange mechanism: displacing a Cu atom upward encounters a barrier of only 0.18 eV [Fig. 4(b)]. The ejected Cu atom diffuses downward by direct hopping over the step with a barrier of 0.62 eV [Fig. 4(c)]. As a result, the Fe atom incorporates into the last atomic row of the upper terrace. The subsequent Fe adatoms approaching the step edge from the lower terrace make the same process, finally leading to the growth of the second embedded row of Fe, one lateral lattice constant away from the step edge [Fig. 4(d)].

Figure 5 clarifies the behavior of the next Fe atoms approaching the step from the lower terrace. The Fe atom [Fig. 5(a)] has to overcome a barrier of 1.02 eV to reach the upper terrace by direct hopping. This transition is suppressed because of the large activation barrier, and the Fe atom incorporates into the step edge by the exchange mechanism with a barrier of 0.34 eV, pushing a Cu atom to the upper terrace [Fig. 5(b)]. The next Fe adatoms approaching the step edge from the lower terrace undergo the same process, leading to the growth of the third row of Fe atoms along the upper terrace [Fig. 5(c)]. The substituted Cu atoms assemble on top of the upper terrace.

Figure 6 demonstrates the behavior of the next Fe atoms approaching the step edge from the lower terrace [Fig. 6(a)]. The Fe atoms move to the upper terrace via the exchange
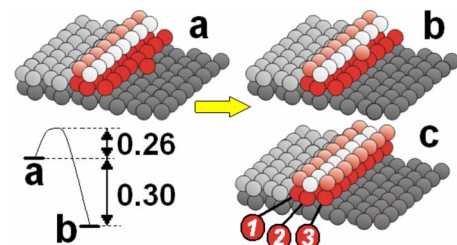

FIG. 6. (Color online) Transition $a \rightarrow b$ is responsible for the growth of the third row of Fe atoms (configuration c) attached to the step edge. The energy differences between the atomic configurations a, b and the value of the activation barrier (in eV) are shown. Red and gray colors represent Fe and Cu atoms, respectively.
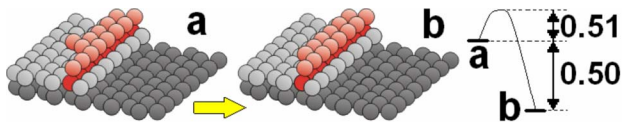
FIG. 7. (Color online) Kink diffusion of Fe atoms near the Fe wire. The energy difference between the atomic configurations and the activation barrier (in eV) are shown. Red and gray colors represent Fe and Cu atoms, respectively.

with an Fe atom of the third embedded row [Fig. 6(b)]. This transition needs an activation energy of 0.26 eV. Subsequent Fe atoms follow the same process, leading to the formation of a new line of Fe atoms on the upper terrace [Fig. 6(c)]. Further, Fe adatoms of the even (the fourth, the sixth, etc.) rows approaching from the lower terrace are uniformly distributed along the step edge due to step-flow diffusion with a barrier of 0.31 eV. At the same time, Fe adatoms of the odd (the fifth, the seventh, etc.) rows approaching from the lower terrace induce the upward mass transport of Fe via exchange mechanism, similar to those demonstrated on Fig. 6 (transition $a \rightarrow b$). This leads to the growth of the bilayer (with respect to the lower terrace) stripe toward the lower terrace in a row-by-row regime.

Now, we discuss the behavior of Fe atoms reaching the step from the upper terrace. Fe atoms diffuse along the Fe nanowire on the upper terrace with a barrier of 0.35 eV. Subsequently approaching Fe atoms form a new row of atoms on the upper terrace. The incorporation of Fe atom into the Fe chain (Fig. 7) requires an activation energy of 0.51 eV. Therefore, the Fe stripe expands onto the upper terrace in a row-by-row fashion. We conclude that Fe stripes grow (increase their width) toward both the lower and upper terraces simultaneously. The speed of growth of Fe on the upper terrace is twice that of the lower terrace because double layers are built on the lower terrace. For equal deposition flux on both terraces, it *looks as if* the stripe grows backward from the edge onto the upper terrace. This explains the observation of Shen *et al.* that the Fe stripe started growth at the upper edge of a terrace and expanded backward.[8] In the light of the present results, this picture is not entirely correct. In the scanning tunneling microscopy experiments, only the actual step edge is seen, not where it was *before* atom deposition.

Figure 8 summarizes our findings and demonstrates the result of the kMC simulation including the full set of atomic processes discussed above. It shows the morphology of a stepped Cu(111) surface after deposition of 0.3 ML of Fe. The formation of regular stripes, 9–11 atoms wide and 1 ML high (with respect to the upper terrace), is observed, in agreement with the experiments.[7,8]

IV. DISCUSSION

In this section, we investigate the role of coverage, temperature, and strain relaxations in the self-organization of atomic Fe stripes on stepped Cu(111).

A. Origin of 1 ML high stripe growth

To explain the origin of 1 ML high stripe formation (with respect to the upper terrace), we examine an Fe atom ap-
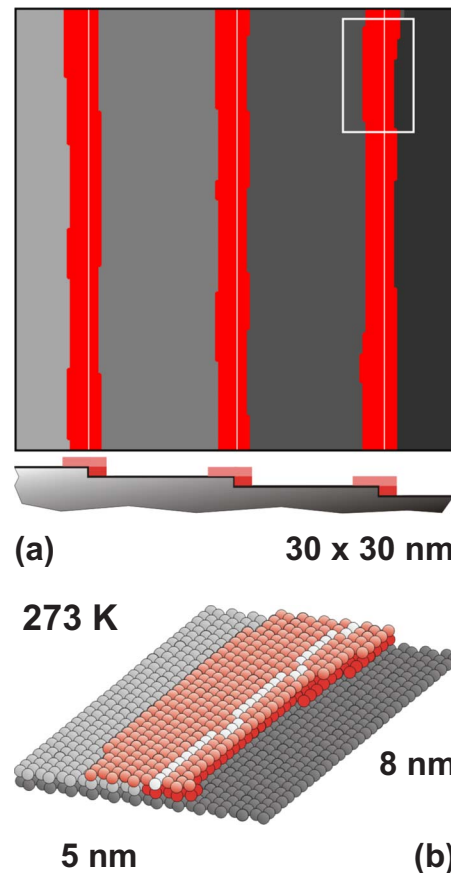

FIG. 8. (Color online) kMC simulation of the morphology of a stepped Cu(111) surface exposed to 0.3 ML of Fe (T=273 K, F =0.2 ML/min). Straight white lines in (a) mark the position of the step edges before the exposure of Fe atoms. Red and gray colors represent Fe and gray atoms, respectively.

proaching the existing stripe (a few atoms wide) from the upper terrace [Fig. 9(a)]. It may induce the upward mass transport to the top of the stripe via exchange mechanism [Fig. 9(b)], but it is unlikely that this transition takes place because of the high energy barrier of 0.88 eV. Moreover, if a deposited Fe atom lands on top of the stripe, it exhibits random diffusion on the top of the stripe with a barrier 0.03 eV. Diffusion of Fe adatom on the Cu(111) surface takes place with a barrier of 0.025 eV. Therefore, a fraction of Cu atoms incorporated into the stripe does not affect the motion of the Fe adatom at 273 K. During random diffusion on top of the stripe, the Fe adatom may approach the stripe edge [Fig. 9(b)], where it may experience downward transport via ex-
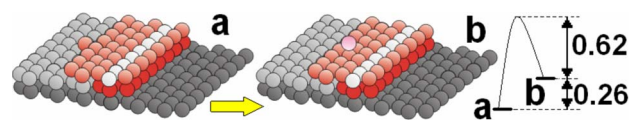

FIG. 9. (Color online) Interlayer diffusion of Fe atoms between the upper terrace and the top of the stripe. The energy difference between the atomic configurations and the activation barrier (in eV) are shown. Red and gray colors represent Fe and Cu atoms, respectively.
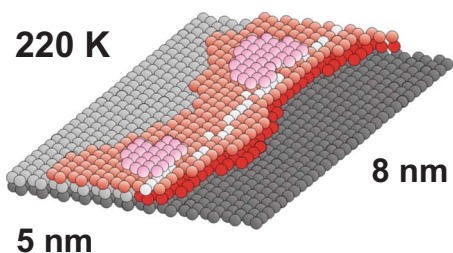
FIG. 10. (Color online) kMC simulation of the morphology of a stepped Cu(111) surface exposed to 0.3 ML of Fe at $T=220$ K ($F=0.2$ ML/min). Red and gray colors represent Fe and Cu atoms.

change with a barrier of 0.62 eV [Fig. 9(a)]. The existence of this atomic mechanism leads to the growth of 1 ML high stripes.

Now, we investigate the behavior of the system when the concentration of deposited Fe is higher than 0.3 ML. Fe atoms may land on top of the stripe during the deposition. When two Fe atoms diffusing meet each other, the formation of dimer takes place. The probability that the Fe atom that landed on top of the stripe would reach its edge [Fig. 9(b)] and would move downward [Fig. 9(a)] decreases with increasing width of the stripe. Therefore, the probability of Fe dimer formation on top of the stripe increases with increasing coverage. The Fe dimer does not dissociate at room temperature, since the binding energy of such dimers is 1.5 eV. Thus, the growth of the second layer takes place. Our kMC simulations indicate that at the considered temperature and flux, the formation of the second layer takes place at $D>0.5$ ML. This finding is consistent with the experimental observation of Shen *et al.*[7,8] and Klaua *et al.*,[45] who have observed a significant fraction of the second Fe layer at coverage of 0.8 and 0.6 ML, respectively.

B. Effect of temperature

Our studies indicate that the temperature of the system is crucial for the self-assembly of well-ordered stripes. Their growth is possible only in a narrow temperature window around 270 K. Decreasing the temperature to 220 K significantly affects the growth process. The result of our kMC simulations is shown in Fig. 10. One can see that the structure that is formed along the step edge has a pronounced fraction in the second layer and exhibits an irregular shape. Its morphology can be explained by the fact that at 220 K, the threshold barrier E_{cr}, which determines whether an atomistic process is operative or not, equals 0.5 eV, i.e., only events with the barriers $E_D < E_{cr}=0.5$ eV are operative. In this situation, the kink diffusion of Fe atoms (Fig. 7), which is responsible for a row-by-row growth regime on the upper terrace, is suppressed. The activation energy for the kink diffusion of Fe atoms on the lower terrace is 0.57 eV. This transition is suppressed as well. As a result, the formation of irregular structures along both upper and lower terraces takes place. Besides, the downward transport of Fe atoms that landed on top of the growing structure is not operative (the barrier is 0.62 eV, Fig. 9), which leads to the formation of the second Fe layer.
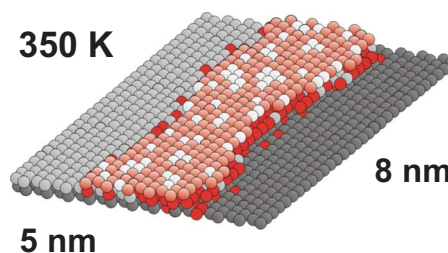

FIG. 11. (Color online) kMC simulation of the morphology of a stepped Cu(111) surface exposed to 0.3 ML of Fe at $T=350$ K ($F=0.2$ ML/min). Red and gray colors represent Fe and Cu atoms.

Increasing the temperature to 350 K significantly affects the growth process as well. The result of our kMC simulations is presented in Fig. 11. One can see that substantial intermixing between the deposited Fe atoms and the Cu substrate takes place. This leads to alloy formation at the interface between the lower and upper terraces. Within our calculations, the barrier for the incorporation of Fe into the Cu substrate is found to be about 1.1 eV. This process is activated at temperatures $T \geq 350$ K. The presence of other Fe impurities embedded into the Cu substrate could reduce the
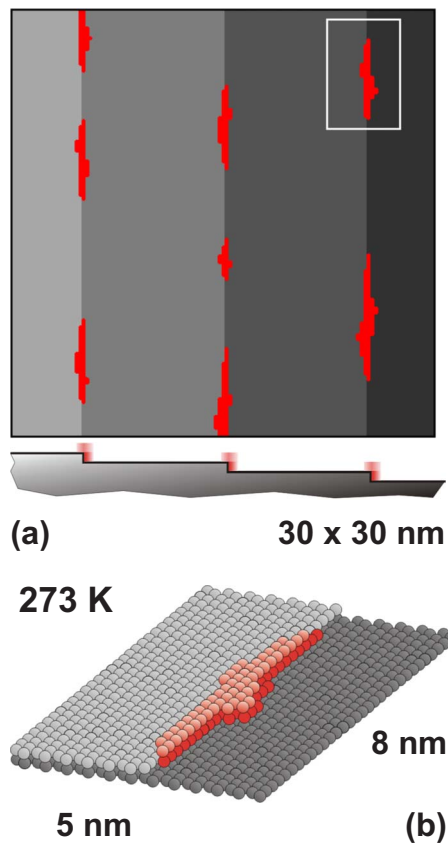

FIG. 12. (Color online) kMC simulation of the morphology of a stepped Cu(111) surface exposed to 0.045 ML of Fe ($T=273$ K, $F=0.2$ ML/min). Strain relaxations are excluded. Snapshot (b) shows the area marked with the white rectangle in (a). Red and gray colors represent Fe and Cu atoms. Obviously, without strain relaxation, only elongated islands form (but not continuous wires).
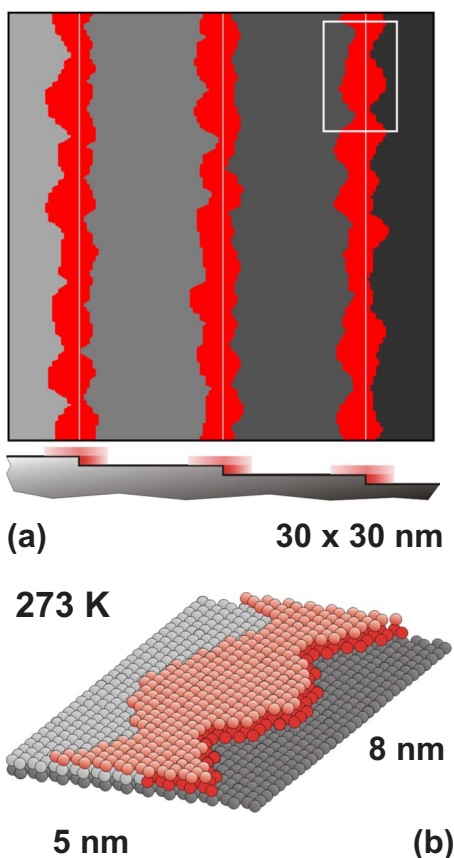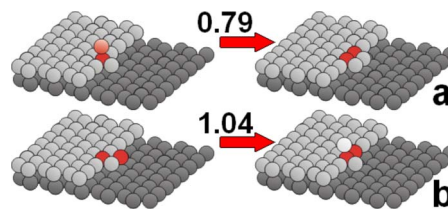
FIG. 14. (Color online) In the absence of strain relaxations, the formation of embedded Fe dimer does not take place independently, whether an Fe atom approaches from the (a) upper or (b) lower terrace. The activation barriers for the corresponding events are given in eV. Red and gray colors represent Fe and Cu atoms.

FIG. 13. (Color online) kMC simulation of the morphology of a stepped Cu(111) surface exposed to 0.3 ML of Fe (T=273 K, F =0.2 ML/min). Strain relaxations are excluded. Consequently, the formation of Fe nanostripes is inhibited. The growing structure (a) has nonuniform density due to different numbers of Fe atoms in the corresponding row. Red and gray colors represent Fe and Cu atoms.

diffusion barrier for incorporation of Fe,[28] leading to stronger intermixing between deposit and substrate.

Another phenomenon that becomes crucial at elevated temperatures (>300 K) is the formation of 1 ML deep Cu holes on the terraces of stepped Cu(111).[45] The relaxation of the Cu substrate near the step edges owing to the tensile stress caused by the Fe nanostructures diminishes the binding energy of substrate Cu atoms of the upper terrace. It results in the enhanced emission of Cu atoms, enabling a mass transport from the eroded parts of the Cu steps to the lower terraces. This process may strongly affect the growth regime and thus must be taken into account at elevated temperatures.[45]

C. Effects of strain relaxation

Previous theoretical and experimental studies have indicated that strain relaxation significantly affects atomic processes near steps. For instance, it has been shown[46] that the strain induced by steps may shift the energy balance between fcc and hcp sites on Cu(111). Strain relaxations affect the shape of the substrate and nanoislands during homo- and heteroepitaxy on Cu(111) (Refs. 23 and 24) and influence

atomic motion near the ascending[25] and descending[26] edges of the nanoislands. Including the size-dependent mesoscopic mismatch is crucial for the understanding of atomic processes in the interlayer mass transport at the edges of nanoislands.[23,24,27] Strain in a Cu(001) substrate affects the energy barriers for atomic exchange around embedded Fe islands and induces collective atomic transitions.[28] Strain is suspected to be the origin of the fast diffusion of small Co clusters on Cu(001).[47] The size-dependent mismatch between Si islands and Si substrate has been also found to be a driving force for surface morphology above percolation.[48] The above results suggest that the relaxations induced in the substrate and in the growing structures could significantly affect the atomic processes during the self-assembly of Fe wires and stripes.

We have artificially excluded strain induced in the Cu substrate and Fe nanostructures and calculated diffusion barriers for all atomic processes for the ideal atomic configurations. Figures 12 and 13 demonstrate the results of kMC simulations: the morphology of a stepped Cu(111) surface at T=273 K covered by 0.045 and 0.3 ML of Fe correspondingly. One can see that in the absence of strain relaxation, growth of monatomic wires and stripes is suppressed.

We have found that in the absence of strain, several atomic processes are not operative anymore. For example, the Fe adatom approaching the clean Cu(111) step edge from the upper terrace incorporates into the step edge with a barrier of 0.10 eV.[49] However, the formation of embedded dimers (and, therefore, longer embedded chains) is inhibited because the barrier for such events is about 0.79 (1.04) eV if the Fe atom approaches the step edge from the upper (lower) terrace (Fig. 14). These barriers are too high. The absence of embedded Fe chains prevents the growth of monatomic Fe wires on top of them. The absence of kink transport of Fe atoms on both lower and upper terraces inhibits the formation of well-ordered stripes.

V. CONCLUSIONS

In summary, we have performed atomic-scale simulations of the growth of Fe nanostripes on a stepped Cu(111) surface. The major atomistic events responsible for the formation of Fe nanostripes have been identified. We have revealed that Fe nanostripes grow (increase their width) toward both upper and lower terraces with different growth speeds. This

looks as if stripe grows backward from the step edge onto the upper terrace. It has been demonstrated that strain relaxation plays a significant role during growth process of 1D Fe nanostructures.

[1] G. F. Newell and E. W. Montroll, Rev. Mod. Phys. **25**, 159 (1953); Rev. Mod. Phys. **25**, 353 (1953).

[2] G. A. Bassett, Philos. Mag. **3**, 1042 (1958).

[3] H. Bethge, Phys. Status Solidi **2**, 775 (1962); Surf. Sci. **3**, 33 (1964).

[4] A. Brodde, K. Dreps, J. Binder, Ch. Lunau, and H. Neddermeyer, Phys. Rev. B **47**, 6609 (1993).

[5] H. J. Elmers, J. Hauschild, H. Höche, U. Gradmann, H. Bethge, D. Heuer, and U. Köhler, Phys. Rev. Lett. **73**, 898 (1994).

[6] Y. W. Mo and F. J. Himpsel, Phys. Rev. B **50**, 7868 (1994); F. J. Himpsel and J. E. Ortega, *ibid.* **50**, 4992 (1994); F. J. Himpsel, J. E. Ortega, G. J. Mankey, and R. F. Willis, Adv. Phys. **47**, 511 (1998) and references therein.

[7] J. Shen, R. Skomski, M. Klaua, H. Jenniches, S. S. Manoharan, and J. Kirschner, Phys. Rev. B **56**, 2340 (1997).

[8] J. Shen, M. Klaua, P. Ohresser, H. Jenniches, J. Barthel, Ch. V. Mohan, and J. Kirschner, Phys. Rev. B **56**, 11134 (1997).

[9] P. Gambardella, M. Blanc, L. Burgi, K. Kuhnke, and K. Kern, Surf. Sci. **449**, 93 (2000).

[10] P. Gambardella, A. Dallmeyer, K. Maiti, M. C. Malagoli, W. Eberhardt, K. Kern, and C. Carbone, Nature (London) **416**, 301 (2002).

[11] Susumu Shiraki, Hideki Fujisawa, Masashi Nantoh, and Maki Kawai, Phys. Rev. Lett. **92**, 096102 (2004); J. Phys. Soc. Jpn. **74**, 2033 (2005).

[12] Y. Mo, K. Varga, E. Kaxiras, and Z. Zhang, Phys. Rev. Lett. **94**, 155503 (2005).

[13] J. Guo, Y. Mo, E. Kaxiras, Z. Zhang, and H. H. Weitering, Phys. Rev. B **73**, 193405 (2006).

[14] X. Tan, G. Ouyang, and G. W. Yang, Appl. Phys. Lett. **88**, 263116 (2006).

[15] M. C. Payne, L. J. Robertson, D. Thomson, and V. Heine, Philos. Mag. B **73**, 191 (1995).

[16] F. Ercolessi and J. B. Adams, Europhys. Lett. **26**, 583 (1994).

[17] G. C. Kallinteris, N. I. Papanicolaou, G. A. Evangelakis, and D. A. Papaconstantopoulos, Phys. Rev. B **55**, 2150 (1997).

[18] Y. Mishin, D. Farkas, M. J. Mehl, and D. A. Papaconstantopoulos, Phys. Rev. B **59**, 3393 (1999).

[19] G. J. Ackland, M. J. Mendelev, D. J. Srolovitz, S. Han, and A. V. Barashev, J. Phys.: Condens. Matter **16**, 2629 (2004).

[20] M. Müller, P. Erhart, and K. Albe, J. Phys.: Condens. Matter **19**, 326220 (2007).

[21] V. Rosato, B. Guillope, and B. Legrand, Philos. Mag. A **59**, 321 (1989); F. Cleri and V. Rosato, Phys. Rev. B **48**, 22 (1993).

[22] V. S. Stepanyuk, A. N. Baranov, D. V. Tsivlin, W. Hergert, P. Bruno, N. Knorr, M. A. Schneider, and K. Kern, Phys. Rev. B **68**, 205410 (2003); V. S. Stepanyuk, A. L. Klavsyuk, W. Hergert, A. M. Saletsky, P. Bruno, and I. Mertig, *ibid.* **70**, 195420 (2004); S. Pick, V. S. Stepanyuk, A. L. Klavsyuk, L. Niebergall, W. Hergert, J. Kirschner, and P. Bruno, *ibid.* **70**, 224419 (2004); R. A. Miron and K. A. Fichthorn, Phys. Rev. Lett. **93**, 128301 (2004); K. Sastry, D. D. Johnson, D. E. Goldberg, and P. Bellon, Phys. Rev. B **72**, 085438 (2005); V. S. Stepanyuk, A. L. Klavsyuk, L. Niebergall, A. M. Saletsky, W. Hergert, and P. Bruno, Phase Transitions **78**, 61 (2005).

[23] O. V. Lysenko, V. S. Stepanyuk, W. Hergert, and J. Kirschner, Phys. Rev. Lett. **89**, 126102 (2002).

[24] V. S. Stepanyuk, D. I. Bazhanov, A. N. Baranov, W. Hergert, P. H. Dederichs, and J. Kirschner, Phys. Rev. B **62**, 15398 (2000).

[25] D. V. Tsivlin, V. S. Stepanyuk, W. Hergert, and J. Kirschner, Phys. Rev. B **68**, 205411 (2003).

[26] V. S. Stepanyuk, D. I. Bazhanov, W. Hergert, and J. Kirschner, Phys. Rev. B **63**, 153406 (2001).

[27] O. V. Lysenko, V. S. Stepanyuk, W. Hergert, and J. Kirschner, Phys. Rev. B **68**, 033409 (2003).

[28] R. C. Longo, V. S. Stepanyuk, W. Hergert, A. Vega, L. J. Gallego, and J. Kirschner, Phys. Rev. B **69**, 073406 (2004).

[29] N. A. Levanov, V. S. Stepanyuk, W. Hergert, D. I. Bazhanov, P. H. Dederichs, A. Katsnelson, and C. Massobrio, Phys. Rev. B **61**, 2230 (2000).

[30] K. Wildberger, V. S. Stepanyuk, P. Lang, R. Zeller, and P. H. Dederichs, Phys. Rev. Lett. **75**, 509 (1995).

[31] V. S. Stepanyuk, W. Hergert, K. Wildberger, R. Zeller, and P. H. Dederichs, Phys. Rev. B **53**, 2121 (1996).

[32] S. L. Dudarev and P. M. Derlet, J. Phys.: Condens. Matter **17**, 7097 (2005); see also Ref. 33.

[33] G. J. Ackland, Phys. Rev. Lett. **97**, 015502 (2006).

[34] G. Kresse and J. Hafner, Phys. Rev. B **48**, 13115 (1993); G. Kresse and J. Furthmüller, Comput. Mater. Sci. **6**, 15 (1996); G. Kresse and D. Joubert, Phys. Rev. B **59**, 1758 (1999).

[35] A fcc hollow site is considered for the case of (111) surface.

[36] F. H. G. Ehrlich, J. Chem. Phys. **44**, 1039 (1966).

[37] R. Schwöebel and E. Shipsey, J. Appl. Phys. **37**, 3682 (1966).

[38] K. A. Fichthorn and W. H. Weinberg, J. Chem. Phys. **95**, 1090 (1991).

[39] A. Bogicevic, J. Strömquist, and B. I. Lundqvist, Phys. Rev. Lett. **81**, 637 (1998); A. Bogicevic, S. Ovesson, P. Hyldgaard, B. I. Lundqvist, H. Brune, and D. R. Jennison, *ibid.* **85**, 1910 (2000).

[40] S. Ovesson, A. Bogicevic, and B. I. Lundqvist, Phys. Rev. Lett. **83**, 2608 (1999); S. Ovesson, A. Bogicevic, G. Wahnström, and B. I. Lundqvist, Phys. Rev. B **64**, 125423 (2001).

[41] K. A. Fichthorn and M. Scheffler, Phys. Rev. Lett. **84**, 5371 (2000); K. A. Fichthorn, M. L. Merrick, and M. Scheffler, Phys. Rev. B **68**, 041404(R) (2003).

[42] J. M. Pomeroy, J. Jacobsen, C. C. Hill, B. H. Cooper, and J. P. Sethna, Phys. Rev. B **66**, 235412 (2002).

[43] M. Müller, K. Albe, C. Busse, A. Thoma, and T. Michely, Phys. Rev. B **71**, 075407 (2005).

[44] To avoid excessive details, we do not demonstrate this event and the corresponding value of the activation barrier in Fig. 4.

[45] M. Klaua, H. Höche, H. Jenniches, J. Barthel, and J. Kirschner, Surf. Sci. **381**, 106 (1997).

[46] M. Giesen and H. Ibach, Surf. Sci. **529**, 135 (2003).

[47] R. A. Miron and K. A. Fichthorn, Phys. Rev. B **72**, 035415 (2005).

[48] R. Dana and Y. Manassen, Europhys. Lett. **79**, 16001 (2007).

[49] For comparison, if strain relaxations are included in calculations, the barrier for the incorporation of Fe atom into the clean descending Cu(111) step B equals 0.08 eV.